Published in final edited form as:

Clin Cancer Res. 2022 April 01; 28(7): 1433–1445. doi:10.1158/1078-0432.CCR-21-2984.

Metabolic Alterations and WNT Signaling Impact Immune Response in HGSOC

Rebecca C. Arend[1], **Carly B. Scalise**[1], **Emily R. Gordon**[2], **Allison M. Davis**[1], **McKenzie E. Foxall**[1], **Bobbi E. Johnston**[2], **David K. Crossman**[3], **Sara J. Cooper**[2]

[1]Department of Obstetrics and Gynecology, University of Alabama at Birmingham, Birmingham, Alabama.

[2]HudsonAlpha Institute for Biotechnology, Huntsville, Alabama.

[3]Department of Genetics, University of Alabama at Birmingham, Birmingham, Alabama.

Abstract

Purpose: Our study used transcriptomic and metabolomic strategies to determine the molecular profiles of HGSOC patient samples derived from primary tumor and ascites cells. These data identified clinically relevant heterogeneity among and within patients and highlighted global and patient-specific cellular responses to neoadjuvant chemotherapy (NACT).

Experimental Design: Tissue from 61 treatment-naïve patients with HGSOC were collected. In addition, 11 benign, 32 ascites, and 18 post-NACT samples (matched to the individual patient's pre-NACT sample) were collected. RNA sequencing (RNA-seq) was performed on all samples collected. Two-dimensional spatial proteomic data was collected for two pairs of pre- and post-NACT. Untargeted metabolomics data using GCxGC-MS was generated for 30 treatment-naive tissues. Consensus clustering, analysis of differential expression, pathway enrichment, and survival analyses were performed.

Results: Treatment-naïve HGSOC tissues had distinct transcriptomic and metabolomic profiles. The mesenchymal subtype harbored a metabolomic profile distinct from the other subtypes. Compared with primary tumor tissue, ascites showed significant changes in immune response and signaling pathways. NACT caused significant alterations in gene expression and WNT activity, and this corresponded to altered immune response. Overall, WNT signaling levels were inversely

Corresponding Author: Rebecca C. Arend, Obstetrics and Gynecology, University of Alabama at Birmingham, 619 19th Street South, Birmingham, AL 35294-0024. Phone: 205-934-7789; rarend@uabmc.edu.
R.C. Arend and C.B. Scalise contributed equally as co-first authors of this article.

Authors' Contributions

R.C. Arend: Conceptualization, resources, supervision, writing–original draft. **C.B. Scalise:** Conceptualization, resources, formal analysis, visualization, methodology, writing–original draft, writing–review and editing. **E.R. Gordon:** Resources, data curation, software, formal analysis, writing–original draft. **A.M. Davis:** Resources, writing–original draft. **M.E. Foxall:** Resources, writing–original draft. **B.E. Johnston:** Data curation, software, formal analysis, writing–original draft. **D.K. Crossman:** Resources, data curation, software, formal analysis, writing–original draft. **S.J. Cooper:** Conceptualization, resources, data curation, software, formal analysis, supervision, funding acquisition, validation, investigation, visualization, methodology, writing–original draft, writing–review and editing.

The costs of publication of this article were defrayed in part by the payment of page charges. This article must therefore be hereby marked *advertisement* in accordance with 18 U.S.C. Section 1734 solely to indicate this fact.

Note: Supplementary data for this article are available at Clinical Cancer Research Online (http://clincancerres.aacrjournals.org/).

correlated with immune cell infiltration in HGSOC tissues and WNT signaling post-NACT was inversely correlated with progression-free survival.

Conclusions: Our study concluded that HGSOC is a heterogenous disease at baseline and growing molecular differences can be observed between primary tumor and ascites cells or within tumors in response to treatment. Our data reveal potential exploratory biomarkers relevant for treatment selection and predicting patient outcomes that warrant further research.

Introduction

High-grade serous ovarian cancer (HGSOC) remains the deadliest gynecologic malignancy with an estimated 21,410 new diagnoses and 13,770 deaths expected in the United States in 2021 (1). Over 80% of patients with HGSOC exhibit response to chemotherapy; however, the majority will develop disease recurrence with inadequate therapeutic response (2). Platinum-resistant (PR) patients have a median survival of 9 to 12 months compared with sensitive counterparts at 24 months (3). Identifying mechanisms that drive PR can translate into therapeutic interventions that would improve patient outcomes.

Currently, there is a significant effort to implement personalized medicine approaches to improve patient outcomes. These approaches include utilization of genomic technologies to characterize gene expression, gene mutations, copy-number changes, and epigenetic reprogramming. RNA sequencing (RNA-seq) is a key genomic technology used to understand molecular pathogenesis in OC (4). RNA-seq of large HGSOC cohorts led to the identification of transcriptomic signatures that correlate with molecular phenotypes and clinical outcomes. The four initial OC transcriptional subtypes identified were differentiated, immunoreactive, mesenchymal, and proliferative (5, 6), followed by a fifth subtype, antimesenchymal (7).

In addition, transcriptional signatures derived from RNA-seq data are being developed in an effort to categorize patients into effective therapies. These signatures assess levels of signaling for WNT (8), mTOR (9), and TGFβ (10) as well as immune cell infiltration (11). The tumor inflammation signature (TIS), also computed from RNA-seq data, quantifies immune activity in the tumor and is correlated with response to immune checkpoint blockade (ICB) therapy and patient survival (12). The link between immune cell infiltration and treatment response is well established and has led to other work linking WNT signaling to the exclusion of effector T immune cells from the tumor (13–15). While RNA-seq gene signatures have been widely studied in HGSOC, metabolic reprogramming has not been well characterized. Metabolic programming is a hallmark of cancer (16, 17) and contributes to chemoresistance, metastatic potential, and immunosuppression (18–20).

In the current study, we describe the heterogeneity found in chemo-naïve HGSOC tissues and how to leverage genomic data in a clinical setting. Importantly, we explore possibility that markers of treatment response might be found in ascites cells and post-treatment tissues, with a particular interest in factors contributing to immune response. Our data show the potential for genomic and metabolomic analyses to identify key signatures of primary tumor and ascites cells, and how treatment response can identify potential therapeutic targets in patients with HGSOC.

Materials and Methods

Sample specimen collection and processing

Under IRB approval between July 2009 and September 2017, tissues from 61 consented individuals with HGSOC were collected in accordance with recognized ethical guidelines: 61 chemo-naïve tissues at the time of either PDS or diagnostic laparoscopy; 32 ascites collected at PDS, diagnostic laparoscopy, or therapeutic paracentesis pre-NACT; 18 matched sets of individual patients' pre- and post-NACT tissues (post-NACT tissue collected at the time of IDS); and 11 benign adnexal masses. All tissue samples tissues were flash frozen or deposited into RNA later (Sigma #R0901) at the time of resection and stored at −80°C until the time of RNA extraction. Cells from ascites fluid were isolated by centrifugation as previously described (21).

Patient demographics and clinical data

Patient demographics and clinical data were obtained from chart review to include age, body mass index (BMI), race, tumor stage, overall and progression-free survival (OS and PFS, respectively), BRCA status, and response to platinum-based treatment. OS was defined as the amount of time from diagnosis to last follow-up for surviving patients or death for deceased patients. PFS was determined as the amount of time, in months, from the initiation of treatment to first recurrence. Platinum sensitivity was determined 6 months after the end of chemotherapy; PS patients did not have evidence of disease progression 6 or more months after treatment ended, whereas PR patients had disease progression within 6 months of the end of treatment.

RNA-seq

We used the Norgen Total RNA Isolation kit (Cat #17200) to isolate RNA. Tissue homogenates (FastPrep, lysing matrix D, MP Bio) were treated with Proteinase K before being applied to the column, and on-column DNAse treatment was done following the manufacturer's instructions. Ascites samples were lysed in RLT before RNA Isolation without homogenization. Total RNA was eluted from the columns and quantified using the Qubit RNA BR Assay Kit and the Qubit 2.0 fluorometer (Invitrogen). The median RNA integrity Number (RIN) values were as follows: tissue samples = 8.35 (2.4–8.9) and ascites = 8.6 (6.1–9.8; Supplementary Table S1). All samples were included in the analysis of pre- and post-NACT, to maximize the number of matched pre- and posttreatment tissues.

Approximately 800 ng of total RNA was used as input to the NEBNext Ultra RNA Library Prep Kit for Illumina using the polyA selection method (E7530S and E7490S). Libraries were barcoded using NEBNext multiplex oligos for Illumina (E7335S). Five samples were pooled per lane on an Illumina HiSeq 2500 flow cell and sequenced an average of 29 M aligned reads per sample and an average quality score of 35 with 93% >Q30. Samples that failed sequencing, resulting in less than 1 M reads, were removed from analysis, yielding our final totals of 61 treatment-naïve samples, 18 platinum-treated tumor samples, 25 ascites samples, and 11 benign tissue samples. All 18 post-NACT and 24 of 25 ascites samples came from one of the patients for which we also collected treatment-naïve tissue and

RNA-seq data. Raw and processed data and full description of alignment tools are available using the GEO Accession GSE143897.

Consensus clustering for subtypes

To calculate consensus clusters using *de novo* analysis of our transcriptomic data, we identified the 1,500 most variable genes as those with the highest variance. *ConsensusClusterPlus()* was run with maxK = 10, clusterAlg = km, bootstraps = 1000, and distance = Euclidean (22). The most stable clusters were when $k = 4$ (Supplementary Table S1).

Transcriptional subtype assignment

Transcriptional subtypes were defined as described in Tothill and colleagues or Wang and colleagues (6, 7). We calculated a *Z*-score across samples for expression of the Tothill and Wang signature genes using the transformed data from varianceStabilizingTransformation(). Then a Pearson correlation was calculated between the subtypes defined by Tothill and Wang and the normalized expression vectors for signature genes in each sample. Each sample was assigned to the subtype for which the Pearson correlation with the defined subtype was highest. Any sample without a correlation exceeding 0.1 was not assigned a subtype ("NA"; Supplementary Table S1).

Differential expression analysis

Differentially expressed genes (DEG) were determined using DESeq2. For analyses that spanned more than one batch of sequencing, batch was used as a covariate in the design model (23). No other covariates (e.g., age or grade) were used in the models because all patients were grade 3–4 and age was not strongly associated with clinical traits. For analysis of pre- and post-NACT and tumor versus ascites samples, a paired analysis that accounts for individual variation was conducted (design ~Patient+Treatment or ~Patient+SampleType).

Metabolomic analysis

Metabolomic analysis was conducted as previously described (24, 25). For all HGSOC tissue samples for which sufficient tissue remained after transcriptomic analysis we extracted metabolites from 100 mg of tissue using 50% methanol. Extracts were derivatized by methoximation and trimethylsilylation and analyzed on a LECO Pegasus 4D system (GCxGC-TOFMS). ChromaTOF 4.51.6 software (Leco) was used for peak calling, deconvolution, and initial library spectra matching. R2DGC was used for peak alignment and metabolite identification (26). Assignments were confirmed manually. Statistical analysis including clustering and differential abundance analysis by ANOVA was done using Metaboanalyst 4.0 (27). Pathway visualization was done using Pathvisio and WikiPathways (28).

Pathway analysis

DESeq2 output contrasting sample type or pre- and post-NACT of all measured transcripts with a $\log_2$fold change and adjusted *P* value were used as input for the pathway analysis tool LRPath in RNAEnrich mode (29). The output yields enrichment for pathways based on

rank correlation and a direction of effect. We plotted the adjusted *P* values of the topmost enriched pathways. For pathway analysis of gene expression modules pre- and post-NACT, GOrilla was used (http://cbl-gorilla.cs.technion.ac.il).

Calculation of pathway activity and immune cell infiltration

We used gene sets (metagenes) with known function or cell-type specificity as a proxy for pathway activity or cell type abundance. The gene sets were derived from the literature (9, 11, 30–32). For each set of genes, we determined the median variance stabilized gene expression value (using the variance stabilized transformation function in DESeq2). The Tumor Inflammation Signature (TIS) was calculated based on a weighted average of the normalized expression of TIS genes using weights identified by Ayers and colleagues, but CCL5 was not included as the transcript is not included in the gene models for hg19 (12). Additional estimates of immune cell subtypes were generated using Cibersort (33).

NanoString GeoMx digital spatial profile analysis

Unstained slides from formalin-fixed paraffin-embedded (FFPE) blocks from 2 patients (included in RNA-seq analysis), pre- and post-NACT, were sent for NanoString (https://www.nanostring.com) GeoMx Digital Spacial Profiling (DSP) Analysis using the Human Immuno-Oncology Protein Panel. This panel allows for multi-plex, high-throughput spatial profiling to quantify and spatially map 70 proteins in both tumor and immune cells simultaneously. DSP provides quantitative protein data from 6 regions of interest (ROI) on each slide. Each region is further divided into tumor ($PanCK^{+}CD45^{-}$) and immune ($PanCK^{-}CD45^{+}$) areas resulting in 6 tumor and 6 immune areas with 70 protein readouts per area, termed tumor segmentation.

Survival analysis

Kaplan–Meier Plotter was used to generate KM curves. We compared outcomes for the top and bottom tertile of expression in patients with stages III or IV HGSOC only (n = 1,023 for OS and n = 1,001 for PFS). We selected “Jet set” probes, as recommended. The probe ID for each gene is noted in the plots. Sources for the database include GEO, EGA, and TCGA (Gene Expression Omnibus, European Genome-phenome Archive, The Cancer Genome Atlas). Website: https://kmplot.com/analysis/.

Statistical analysis

R version 4.0.0 was used for all other statistical analysis unless described otherwise above. The following general packages were used: gplots, limma, dplyr, and ggplot2. ComplexHeatmap package with Spearman as the distance metric was used for heatmaps. Survplot and survminer were used to generate KM curves and calculate Cox proportional hazard ratios (https://github.com/kassambara/survminer). For matched tissues (tumor pre- and post-NACT tissues), we calculated a normalized $\log_2$fold change and calculated hazard ratios associated with those changes using the coxph() function.

Data availability

The data that support the findings of this study are available from the corresponding author, RCA, upon reasonable request.

Results

HGSOC tissues harbor transcriptional and metabolic heterogeneity

To determine the transcriptional differences in tumor and benign tissue, we performed RNA-seq on 61 chemo-naïve II–IV HGSOC tissues and 11 benign tissues; a summary of patient demographics and clinical characteristics are shown in Table 1. We identified 10,817 DEGs between the tumor and benign tissues (FDR < 0.01; Supplementary Fig. S1A). Pathway analysis of the DEGs revealed enrichment for genes involved in cell cycle and cell division (Supplementary Fig. S1B). Next, we performed consensus clustering on the 61 HGSOC tissues using the top 1,500 most variable genes to compare gene expression patterns across the tumor tissues, identifying four reproducible clusters (Supplementary Fig. S2). When comparing each cluster's gene expression profile to previously defined transcriptional subtypes (6, 7), we determined that our *de novo*–defined clusters could be mapped to previously defined subtypes (Fig. 1A). Consensus clusters 1 and 2 associated with mesenchymal (M) and immunoreactive (I) subtypes; cluster 3 with immunoreactive (I) subtype; and cluster 4 with proliferative subtype (Fig. 1A). While not statistically significant, proliferative (P) and differentiated (D) subtypes had improved OS compared with the other subtypes (Fig. 1B; Supplementary Fig. S3) with consensus cluster 1 having the worst OS (Fig. 1C). These results are consistent with previously published data confirming HGSOC patients with mesenchymal or immunoreactive tumor profiles have worse survival outcomes compared with proliferative tumors.

Next, we used untargeted metabolomics to measure 130 metabolites from 30 of the 61 chemo-naïve HGSOC tissues for which sufficient tissue was available. Because of the limited sample number, we did not use *de novo* clustering in this analysis. Instead, we identified altered metabolite levels associated with subtypes assigned based on transcriptomics (Fig. 1D). We observed that metabolite profiles from samples assigned to mesenchymal (M) subtype stood out as being like one another but different from other tissues we profiled. An integration of gene expression and metabolite differences in mesenchymal (M) subtype showed significant metabolic changes related to energy metabolism (Fig. 1E). Glucose, pyruvate, asparagine, and glutamine were among the metabolites significantly increased ($P < 0.05$) in mesenchymal (M) compared with other transcriptional subtypes (Fig. 1E). Of the genes involved in synthesis or processing of glucose or glutamine metabolites, we identified PDK4 and GLS that were upregulated in mesenchymal subtype and whose increased expression corresponded to worse PFS among patients in an independent, publicly available dataset (Fig. 1F and G; $P < 0.05$ and $P < 0.001$, respectively). We explored what signaling pathways could be behind the altered metabolic phenotype in this subtype and found a subset of genes regulated by mTOR and PPARG whose expression were elevated.

Identification of treatment-relevant genomic features in HGSOC tumors

To identify treatment-relevant genomic features in our 61 chemo-naïve HGSOC patients, we used previously defined gene sets (metagenes) to estimate activity of key pathways with known therapeutic targets in HGSOC (Fig. 2A; refs. 34–36). Increased MAPK signaling (green ■) and markers of high rate of proliferation (blue ■) were the most common features followed by mTOR signaling (red ■) and immune infiltration (yellow ■; Fig. 2A). The mTOR and MAPK signaling pathways are common targets in cancer therapeutics, but have not been approved for primary OC. Furthermore, HGSOC is characterized by chromosomal instability caused by homologous recombination repair pathway deficiency (HRd; ref. 37). The presence of HRd in HGSOC is a biomarker of poly (ADP-ribose) polymerase inhibitor (PARPi) sensitivity (37). PARPi's are used to treat recurrent/chemoresistant OC patients with tumor gene signatures related to "BRCAness" or $BRCA^{+}$ because they effectively kill these tumor cells regardless of the underlying mechanism of HRd (38). A small percentage (13%) of patients (including 3 that were known to have *BRCA* mutations) had transcriptional signatures associated with "BRCAness" (pink ■) suggesting response to PARPi (Fig. 2A).

In our patient cohort, 14 patients did not have a gene signature associated with response to an existing therapy. We compared gene expression from these 14 patients to the rest of the cohort and identified DEGs, and among them, ADH1B had a significant increase ($P < 0.001$) in expression in these 14 patients. Elevated ADH1B expression corresponded to decreased OC patient PFS (Fig. 2B). More globally, we used pathway analysis to characterize the set of genes differentially expressed in this group of patients and found enrichment for pathways involved in immune response and activation (Fig. 2C). Six of the patients were assigned the immunological transcriptional subtype. They had intermediate levels of T-cell infiltration and did not meet the cut-off we used but have similar, albeit somewhat lower signatures, of immune cell infiltration. These patients may benefit from a treatment that would enhance the immune response.

Research has highlighted multiple signaling pathways, including MAPK and mTOR, that contribute to immune responses in TME (39, 40), and we have observed an increase in T-cell infiltration and antitumor responses in OC treated with WNT pathway inhibitors (13, 14, 41). We estimated the activity of these three pathways using the expression of published target genes to determine whether they correlated with levels of T-cell infiltration in our 61 chemo-naïve tumor tissues. No significant correlation was observed between the MAPK ($P = 0.19$) or mTOR ($P = 0.50$) signaling activity and T-cell infiltration (Fig. 2D). However, activity of the WNT pathway was inversely correlated ($P < 0.001$) with T-cell infiltration in the tumors (Fig. 2D). Next, we tested the WNT pathway's effects on infiltration of other immune cell subsets using expression of cell-type specific genes from the bulk RNA-seq data (11, 33). We determined that WNT signaling is inversely correlated with infiltration of cytotoxic cells ($P < 0.001$), natural killer (NK) cells ($P < 0.001$), and M1 macrophages ($P < 0.05$; Fig. 2E).

Prognostic markers derived from ascites cells include WNT signaling and immune response genes

Advanced-stage HGSOC can have an accumulation of ascites fluid in the peritoneal cavity (Fig. 3A). Furthermore, tumor-derived cells present in ascites are thought to be stem-like, thus contributing to therapeutic resistance (42). In our analyses, we collected matched patient primary tumor tissue with ascites fluid ($n = 32$). We determined the transcriptional subtype of each ascites sample and compared it with the subtype of the individual patient's matched primary tumor tissue. Only 37% ($n = 12$) of patients had matched ascites and primary tumor with the same transcriptional subtype (Fig. 3B). The most common transcriptional subtype found in ascites was mesenchymal (M; 25%; Fig. 3B). This result is in concordance with previous studies showing that ascites fluid contains a subset of resistant, more mesenchymal-like cells (43). Given the lack of consistency between transcriptional subtypes within a patient, we sought to understand whether there were common profiles/pathways that might target both primary tumor and ascites cells. We generated RNA-seq data from ascites cells and compared it to RNA-seq data from matched chemo-naïve primary tumor tissues and found 10,596 genes that were significantly different ($P < 0.05$; Fig. 3C). Many of these differences can be accounted for by differences in the cellular composition of the primary tumor compared with the ascites, along with ascites composition of tumor cells and erythrocytes, leukocytes, fibroblasts, and other nontumor cells. DEGs overexpressed in ascites showed enrichment in pathways involved in translation (GO: 0006412; $P < 10^{-50}$), energy metabolism (GO:0046034, $P < 10^{-41}$), and immune response (GO: 0002220; $P < 10^{-14}$) compared with primary tumor tissue. In addition, we found that high WNT signaling scores derived from ascites cell expression inversely correlated with patient PFS ($P < 0.05$; Fig. 3D), and this was linked with low tumor-infiltrating lymphocyte (TIL) scores impairing PFS (Fig. 3E) in these patients. We and others have shown that elevated WNT signaling can suppress effector T-cell function (13–15), and these data suggest that WNT signaling could be a therapeutic target in both ascites and primary tumor to enhance effector T-cell function.

Chemotherapy alters transcriptional profiles and immune responses in HGSOC

Most patients diagnosed with HGSOC are treated with a platinum-based chemotherapy either in the adjuvant (ACT) or neoadjuvant (NACT) setting. With the transcriptional heterogeneity observed across chemo-naïve HGSOC tissues and ascites, we next wanted to characterize molecular responses to chemotherapy. The objective of this analysis was to determine whether pretreatment heterogeneity or the change in expression following treatment could be relevant for predicting treatment response or survival outcomes. We generated RNA-seq data from pre- and matched post-NACT tissue from 18 patients (Fig. 4A). Only 39% ($n = 7$) of patients maintained their transcriptional subtype in response to NACT (Fig. 4B). There was no clear prediction of whether a patient would be PS or PR based on transcriptional subtypes pre- or post-NACT.

A paired analysis of pre- and post-NACT samples revealed 496 DEGs (FDR < 0.05; Fig. 4C). Among these DEGs, ARX/FLJ13058, ATP6V0D2, RERGL, and PLD5 were among the top increased in response to NACT, and their elevated expression corresponded to unfavorable prognoses for OC patients (Supplementary Fig. S4). We assessed whether changes in individual gene expression in response to NACT were linked to patient survival

outcomes (OS and PFS). Increased expression of *VAMP3* and decreased expression of *MTHFD1L* are significantly associated with improved OS ($P = 0.0033$ and $P = 0.016$, respectively; Supplementary Fig. S5A). In addition, increased expression of *SMIM13* and decreased expression of *NEK11* were associated with improved PFS ($P = 0.0022$ and $P = 0.00036$, respectively; Supplementary Fig. S5B). These results highlight several potential therapeutic targets that could be considered in the development of new strategies to improve OC patient survival, highlighting an immediate action that could be taken during a patient's treatment to aid in clinical management.

Given the previously described link between WNT signaling and immune response in primary tumor tissue and ascites, we expected to observe an association with patient outcomes. We found that patients with HGSOC with high WNT activity pre-NACT were more likely to develop PR compared with patients with low WNT activity associated with PS (Fig. 4D). In addition, patients with high WNT activity post-NACT tumors had significantly worse ($P < 0.05$) PFS survival compared with patients with low WNT activity (7.22m–17.83m, respectively; Fig. 4E). Pathway analysis showed that pathways involved in immune response (GO:0006955, $P < 10^{-30}$) and regulation of immune system process (GO:0002682; $P < 10^{-30}$) were enriched post-NACT (Fig. 4F). Immune cell types were estimated from bulk RNA-seq data as described previously (11), and we found that only the M0 (inactive) macrophage population increased in abundance in response to NACT (Fig. 4G). From a list of over 300 known cytokines we found that IL31 and IFNA7 are most correlated with M0 abundance in our cohort ($R = 0.67$ and 0.65, Pearson). The signals driving the increased M0 abundance could be important for understanding a positive immune response to treatment.

We selected two patients with matched pre- and post-NACT tissue for proteomic analysis; 1 patient was PS (Sample ID #36) and 1 patient was PR (Sample ID #22; Fig. 4B). Using the NanoString GeoMx Digital Spatial Profiler (DSP) Analysis platform, we quantified abundance and spatial orientation of >70 cancer-relevant proteins (Supplementary Fig. S6A). This analysis allowed for tumor segmentation of multiple ROIs on each patient tissue that were separated into tumor and immune cells using PanCK and CD45 markers, respectively (Supplementary Fig. S6B and S6C).

The proteomic analysis revealed an increase in immune exhaustion markers in response to NACT in our PR patient that was not observed in PS patient (Fig. 5). Of note, this patient had high WNT signaling at baseline (pre-NACT; Fig. 5A). When analyzing immune proteins of interest, we found this patient had a significant increase in indoleamine-pyrrole 2,3-dioxygenase 1 (IDO1) and T-cell immunoglobulin and mucin domain-containing protein 3 (Tim-3) in response to NACT (Fig. 5A). Furthermore, this patient had a significant increase in general Mϕ (CD68) and T-cell (CD3) markers in response to NACT (Fig. 5A). NACT increased beta-2-microglobulin (B2M/β−2-m), stimulator of interferon genes (STING), and B-cell lymphoma-2 (Bcl-2) in this patient (Fig. 5A). These results complement the change in transcriptional subtype seen in this patient in response to NACT (proliferative to immunoreactive, respectively; Fig. 4B). Our transcriptomic analysis largely agreed with the proteomic data. Of the 16 differentially expressed proteins in this patient, 100% of transcripts were changed in the same direction.

The PS patient had and an immune landscape characterized by proliferation, memory T cell, myeloid activation, and B-cell markers (Fig. 5B). This patient also had significantly higher nuclear protein 67 (Ki67) and memory T-cell marker (CD45RO) in immune-positive cells at baseline in addition to low WNT signaling (Fig. 5B). In addition, this patient had a significant increase in tumor suppressor (p53) and proapoptotic marker (BIM) on tumor-positive cells in response to NACT (Fig. 5B). These results complement the change in transcriptional subtype seen in this patient in response to NACT (proliferative to mesenchymal, respectively; Fig. 4B). Altogether, these results point toward a relationship between WNT signaling, macrophages, immune evasion, and PR.

Discussion

The treatment of OC will continue to increase its reliance on genomic profiles and transcriptomic patterns (44). Current genomic data reported in large, validated datasets, such as TCGA, utilize treatment-naïve HGSOC tissues with limited data available from post-treatment matched tissues or matched ascites. The objectives of this study were to (i) determine how transcriptomic profiles in the tumor vary across the same tissue type, (ii) compare metabolic profiles of chemo-naïve tissues, (iii) compare ascites and primary tumor tissue from the same patient, and (iv) characterize individual response to NACT with the long-term goals of improving our ability to choose a treatment and measure its effectiveness.

When we assigned previously characterized transcriptional subtypes: anti-mesenchymal, mesenchymal, differentiated, immunoreactive, and proliferative subtypes to our cohort of 61 chemo-naïve tissues we did not observe a strong statistical difference in survival outcomes. The relatively small size of our cohort likely contributed to discrepancy in the correlation between molecular subtypes and survival outcomes compared to previously published data. Other groups have reported inconsistencies in the assignment of transcriptional subtypes in part due to heterogeneity within a tumor, including a report that a single tumor may harbor cells of multiple different subtypes (45). For example, *de novo* cluster 1 associated with the mesenchymal and immunoreactive transcriptional subtypes, and had worse prognoses compared to other groups. Throughout this manuscript, the trend behind mesenchymal and immunoreactive genotypes and phenotypes having worse survival outcomes in HGSOC could be interlinked by a particular signaling pathway.

A novel aspect of our study was the integration of metabolomic and transcriptomic data which showed the mesenchymal subtype had notable differences in metabolite expression compared to other subtypes. Analysis of large cohorts like TCGA have shown that mesenchymal subtypes of a variety of cancers have signatures of altered metabolism. Of the genes we identified enriched in mesenchymal transcriptional subtype included PDK4 and GLS, PDK4 was found to promote alternatively activated macrophage (M2 macrophage) polarization (46) and GLS was found to activate M2 macrophages (47). Macrophages can be polarized into an M1- (antitumor) or M2-like (protumor) state, and a high M2:M1 ratio is associated with shorter OC patient survival (48). These data suggest that tumors characterized as mesenchymal could be sensitive to therapies targeting M2 macrophages. Given these results, further investigation of metabolic changes in ascites and/or post-NACT tissues could be revealing in the future.

In OC, there are limited, predictive biomarkers used to determine therapeutic response, one being HRd. HRd is best measured using germline DNA sequencing for known HRd genes (e.g., BRCA1 and BRCA2) or somatic tumor profiling that measures telomeric imbalance, loss of heterozygosity, and large-scale copy-number changes (37). These features are more difficult to detect using RNA-seq data, although transcriptional signatures associated with BRCA gene activity have been described (38). With the goal of identifying additional patients that could benefit from targeted therapies, we determined that many patients in our cohort had tumor gene expression profiles associated with targetable pathways, including, MAPK, mTOR, and WNT. While these pathways have therapies that target their signaling components, there are no FDA-approved therapies that target these pathways in OC. Patients who did not have tumor gene expression profiles associated with an existing therapy had elevated *ADH1B*, and studies have shown that ADH1B enhances OC infiltration and metastasis, and is a marker of residual disease (49). In addition, we found that these patients had elevated pathways in immune response and activation. Additional investigation is warranted to more thoroughly characterize the immune profiles of these patients to determine if an immune-modulating or other targeted therapy would be clinically beneficial. Consistent with previously published data from our group, WNT signaling was negatively associated with T-cell infiltration and signatures of cytotoxic T cells, NK cells, and M1 macrophages. These data support the idea that inhibition of WNT signaling might be a viable option to target in primary tumor to decrease chemotherapy-induced immune cell evasion and/or increase sensitivity to immune checkpoint blockade (ICB) therapy.

Ascites fluid is known to contribute to patient mortality by facilitating metastasis and contributing to therapeutic resistance. Our analysis comparing chemo-naïve tumor tissue and ascites cells from the same patient showed significant differences in transcriptional profiles including changes in transcriptional subtypes. We found that the most common transcriptional subtype in the ascites was the mesenchymal subtype. Studies have shown that cancer stem cells (CSC) have an EMT-like phenotype (50), which can secrete cytokines including IL6, IL8, and IL1β (51) that significantly contribute to an immunosuppressive TME (52–55). In our analysis, we found that ascites with high WNT signaling activity and low TIL infiltration had worse PFS. WNT signaling has been implicated in CSC behavior, immune evasion, and chemoresistance. Furthermore, WNT signaling can also promote macrophage polarization towards an M2-like state (56), and these macrophages can support immune evasion through IDO that is associated with poor prognosis in OC (57). Lastly, M2 macrophage-derived WNT ligand enriches aldehyde dehydrogenase (ALDH) activity within stem-like cell niches (e.g., ascites), and in turn, these cells secrete more WNT ligand to enhance M2 macrophage activity (58).

Studies have shown that platinum-based chemotherapy enriches CSCs in OC (59), and induces local immune activation, which can increase immunogenicity of immune-excluded “cold” OC tumors (60). In HGSOC, enhanced TILs and T-cell activation post-NACT increases platinum-free interval (PFI) >6 months and therapeutic responses to NACT, respectively (61, 62). In our analysis comparing matched, pre- to post-NACT tumor tissues from patients with HGSOC, we found that NACT caused transcriptional subtype switching in over 61% ($n = 11$) of patients. Although this suggests the transcriptional subtypes may fluctuate, the post-NACT samples are taken shortly after a strong treatment regime is

completed, so it is possible that the steady state profiles would be different. *MTHFD1L* and *NEK11* expression were increased in response to NACT. MTHFD1L is a known promoter of tumor progression, associated with poor survival (63), and NEK11 leads to drug resistance in OC (64). Pathways involved in immune response and activation were enriched post-NACT, suggesting that immune-modulating agents could also be useful in this setting. HGSOC patients with high WNT activity post-NACT had worse PFS suggesting WNT signaling inhibition could be beneficial in combination with NACT, or in the post-NACT setting. We noted that infiltration of several immune cell types was negatively correlated with WNT signaling activity, suggesting that inhibition of WNT signaling might improve immune cell response and perhaps recognition of tumor cells during NACT. When we compared immune function in response to NACT between a PR versus PS patient, we found that the PR patient had increased immune exhaustion in response to NACT whereas a PS patient did not. Of note, the PR patient had high WNT signaling pre-NACT, whereas our PS patient had low WNT signaling. Furthermore, the PR patient had increased IDO1 and Tim-3 expression in response to NACT, and IDO1 is commonly found on M2 macrophages and Tim-3 is expressed on Tregs; both contribute to immune evasion. Altogether our data show that HGSOC is a heterogenous disease with WNT signaling a major suppressor of M1 macrophage infiltration into the TME, leading to an M2 macrophage-mediated pro-immune landscape corresponding to platinum resistance and impaired patient survival.

Conclusion

Our transcriptomic and metabolomic analyses provide novel perspectives into characteristics of HGSOC baseline heterogeneity, markers of patient prognosis from primary tumor and ascites, and responses to chemotherapy that could aid in identification of patients with improved outcomes. While prognostic value has been observed in subtyping of treatment-naïve tissue, analysis of ascites samples likely provides additional, independent information. We showed here that WNT signaling, and immune cell infiltration can be markers of prognosis in both tissue sources. Our work highlights some of the challenges in identifying precision medicine approaches for HGSOC patients but it also provides hope in the form of novel therapeutic targets and new avenues to explore to achieve improved outcomes for patients with HGSOC.

Supplementary Material

Refer to Web version on PubMed Central for supplementary material.

Acknowledgments

First, we wish to especially thank all the women who provided tissue samples to this study. We would like to thank all members of the Arend, Cooper, and Myers labs and especially Elizabeth Ramsey for help with acquiring data and Ryne Ramaker for advice about data analysis. E.R. Gordon and S.J. Cooper were supported by the State of Alabama's Cancer Research Funds and HudsonAlpha's Tie the Ribbons Fund for Breast and Ovarian Cancer Research. R.C. Arend and C.B. Scalise were supported by Department of Defense Early Career Investigator Award (W81XWH-18-1-0231).

Authors' Disclosures

R.C. Arend reports grants from Department of Defense during the conduct of the study, as well as nonfinancial support from Leap Therapeutics, AstraZeneca, GSK, Merck, VBL Therapeutics, and Caris Life Sciences outside

the submitted work. C.B. Scalise reports grants from Department of Defense during the conduct of the study. No disclosures were reported by the other authors.

References

1. Cancer facts & figures 2021. 2021. Available from: https://www.cancer.org/content/dam/cancer-org/research/cancer-facts-and-statistics/annual-cancer-facts-and-figures/2021/cancer-facts-and-figures-2021.pdf.
2. Sato S, Itamochi H. Neoadjuvant chemotherapy in advanced ovarian cancer: latest results and place in therapy. Ther Adv Med Oncol 2014;6:293–304. [PubMed: 25364394]
3. Davis A, Tinker AV, Friedlander M. "Platinum resistant" ovarian cancer: what is it, who to treat and how to measure benefit? Gynecol Oncol 2014;133:624–31. [PubMed: 24607285]
4. Wang J, Dean DC, Hornicek FJ, Shi H, Duan Z. RNA sequencing (RNA-Seq) and its application in ovarian cancer. Gynecol Oncol 2019;152:194–201. [PubMed: 30297273]
5. The Cancer Genome Atlas Research Network. Integrated genomic analyses of ovarian carcinoma. Nature 2011;474:609–15. [PubMed: 21720365]
6. Tothill RW, Tinker AV, George J, Brown R, Fox SB, Lade S, et al. Novel molecular subtypes of serous and endometrioid ovarian cancer linked to clinical outcome. Clin Cancer Res 2008;14:5198–208. [PubMed: 18698038]
7. Wang C, Armasu SM, Kalli KR, Maurer MJ, Heinzen EP, Keeney GL, et al. Pooled clustering of high-grade serous ovarian cancer gene expression leads to novel consensus subtypes associated with survival and surgical outcomes. Clin Cancer Res 2017;23:4077–85. [PubMed: 28280090]
8. Goyal L, Sirard C, Schrag M, Kagey MH, Eads JR, Stein S, et al. Phase I and biomarker study of the Wnt pathway modulator DKN-01 in combination with gemcitabine/cisplatin in advanced biliary tract cancer. Clin Cancer Res 2020;26:6158–67. [PubMed: 32878766]
9. Laplante M, Sabatini DM. Regulation of mTORC1 and its impact on gene expression at a glance. J Cell Sci 2013;126:1713–9. [PubMed: 23641065]
10. Gagno S, Poletto E, Bartoletti M, Quartuccio L, Romualdi C, Garziera M, et al. A TGF-beta associated genetic score to define prognosis and platinum sensitivity in advanced epithelial ovarian cancer. Gynecol Oncol 2020;156:233–42. [PubMed: 31711657]
11. Danaher P, Warren S, Dennis L, D'Amico L, White A, Disis ML, et al. Gene expression markers of tumor infiltrating leukocytes. J Immunother Cancer 2017;5:18. [PubMed: 28239471]
12. Ayers M, Lunceford J, Nebozhyn M, Murphy E, Loboda A, Kaufman DR, et al. IFN-gamma-related mRNA profile predicts clinical response to PD-1 blockade. J Clin Invest 2017;127:2930–40. [PubMed: 28650338]
13. Doo DW, Meza-Perez S, Londoño AI, Goldsberry WN, Katre AA, Boone JD, et al. Inhibition of the Wnt/beta-catenin pathway enhances antitumor immunity in ovarian cancer. Ther Adv Med Oncol 2020;12:1758835920913798. [PubMed: 32313567]
14. Goldsberry WN, Meza-Perez S, Londoño AI, Katre AA, Mott BT, Roane BM, et al. Inhibiting WNT ligand production for improved immune recognition in the ovarian tumor microenvironment. Cancers 2020;12:766.
15. Wall JA, Meza-Perez S, Scalise CB, Katre A, Londoño AI, Turbitt WJ, et al. Manipulating the Wnt/beta-catenin signaling pathway to promote anti-tumor immune infiltration into the TME to sensitize ovarian cancer to ICB therapy. Gynecol Oncol 2021;160:285–94. [PubMed: 33168307]
16. De Francesco EM, Sotgia F, Lisanti MP. Cancer stem cells (CSCs): metabolic strategies for their identification and eradication. Biochem J 2018;475:1611–34. [PubMed: 29743249]
17. Hanahan D, Weinberg RA. The hallmarks of cancer. Cell 2000;100:57–70. [PubMed: 10647931]
18. Abramov Y, Carmi S, Anteby SO, Ringel I. Characterization of ovarian cancer cell metabolism and response to chemotherapy by (31)p magnetic resonance spectroscopy. Oncol Res 2013;20:529–36. [PubMed: 24063283]
19. Han CY, Patten DA, Richardson RB, Harper M-E, Tsang BK. Tumor metabolism regulating chemosensitivity in ovarian cancer. Genes Cancer 2018;9:155–75. [PubMed: 30603053]
20. Sun L, Yang X, Yuan Z, Wang H. Metabolic reprogramming in immune response and tissue inflammation. Arterioscler Thromb Vasc Biol 2020;40:1990–2001. [PubMed: 32698683]

21. Arend RC, Londoño-Joshi AI, Samant RS, Li Y, Conner M, Hidalgo B, et al. Inhibition of Wnt/beta-catenin pathway by niclosamide: a therapeutic target for ovarian cancer. Gynecol Oncol 2014;134:112–20. [PubMed: 24736023]
22. Wilkerson MD, Hayes DN. ConsensusClusterPlus: a class discovery tool with confidence assessments and item tracking. Bioinformatics 2010;26:1572–3. [PubMed: 20427518]
23. Love MI, Huber W, Anders S. Moderated estimation of fold change and dispersion for RNA-seq data with DESeq2. Genome Biol 2014;15:550. [PubMed: 25516281]
24. Dunn WB, Broadhurst D, Begley P, Zelena E, Francis-McIntyre S, Anderson N, et al. Procedures for large-scale metabolic profiling of serum and plasma using gas chromatography and liquid chromatography coupled to mass spectrometry. Nat Protoc 2011;6:1060–83. [PubMed: 21720319]
25. Tran TB, Bergen PJ, Creek DJ, Velkov T, Li J. Synergistic killing of polymyxin B in combination with the antineoplastic drug mitotane against polymyxin-susceptible and -resistant acinetobacter baumannii: a metabolomic study. Front Pharmacol 2018;9:359. [PubMed: 29713282]
26. Ramaker RC, Gordon ER, Cooper SJ. R2DGC: threshold-free peak alignment and identification for 2D gas chromatography-mass spectrometry in R. Bioinformatics 2018;34:1789–91. [PubMed: 29280991]
27. Chong J, Soufan O, Li C, Caraus I, Li S, Bourque G, et al. MetaboAnalyst 4.0: towards more transparent and integrative metabolomics analysis. Nucleic Acids Res 2018;46:W486–94. [PubMed: 29762782]
28. van Iersel MP, Kelder T, Pico AR, Hanspers K, Coort S, Conklin BR, et al. Presenting and exploring biological pathways with PathVisio. BMC Bioinf 2008;9:399.
29. Kim JH, Karnovsky A, Mahavisno V, Weymouth T, Pande M, Dolinoy DC, et al. LRpath analysis reveals common pathways dysregulated via DNA methylation across cancer types. BMC Genomics 2012;13:526. [PubMed: 23033966]
30. Konstantinopoulos PA, Spentzos D, Karlan BY, Taniguchi T, Fountzilas E, Francoeur N, et al. Gene expression profile of BRCAness that correlates with responsiveness to chemotherapy and with outcome in patients with epithelial ovarian cancer. J Clin Oncol 2010;28:3555–61. [PubMed: 20547991]
31. Luke JJ, Bao R, Sweis RF, Spranger S, Gajewski TF. WNT/beta-catenin pathway activation correlates with immune exclusion across human cancers. Clin Cancer Res 2019;25:3074–83. [PubMed: 30635339]
32. Wagle M-C, Kirouac D, Klijn C, Liu B, Mahajan S, Junttila M, et al. A transcriptional MAPK Pathway Activity Score (MPAS) is a clinically relevant biomarker in multiple cancer types. NPJ Precis Oncol 2018;2:7. [PubMed: 29872725]
33. Newman AM, Steen CB, Liu CL, Gentles AJ, Chaudhuri AA, Scherer F, et al. Determining cell type abundance and expression from bulk tissues with digital cytometry. Nat Biotechnol 2019;37:773–82. [PubMed: 31061481]
34. Arend RC, Londoño-Joshi AI, Straughn JM, Buchsbaum DJ. The Wnt/beta-catenin pathway in ovarian cancer: a review. Gynecol Oncol 2013;131:772–9. [PubMed: 24125749]
35. Ediriweera MK, Tennekoon KH, Samarakoon SR. Role of the PI3K/AKT/mTOR signaling pathway in ovarian cancer: Biological and therapeutic significance. Semin Cancer Biol 2019;59:147–60. [PubMed: 31128298]
36. Alzahrani AS. PI3K/Akt/mTOR inhibitors in cancer: at the bench and bedside. Semin Cancer Biol 2019;59:125–32. [PubMed: 31323288]
37. Takaya H, Nakai H, Takamatsu S, Mandai M, Matsumura N. Homologous recombination deficiency status-based classification of high-grade serous ovarian carcinoma. Sci Rep 2020;10:2757. [PubMed: 32066851]
38. Kondo T, Kanai M, Kou T, Sakuma T, Mochizuki H, Kamada M, et al. Impact of BRCAness on the efficacy of oxaliplatin-based chemotherapy in patients with unresectable pancreatic cancer. J Clin Oncol 2017;35:250.
39. Peng W, Chen JQ, Liu C, Malu S, Creasy C, Tetzlaff MT, et al. Loss of PTEN promotes resistance to T cell-mediated immunotherapy. Cancer Discov 2016;6:202–16. [PubMed: 26645196]
40. Conciatori F, Bazzichetto C, Falcone I, Pilotto S, Bria E, Cognetti F, et al. Role of mTOR signaling in tumor microenvironment: an overview. Int J Mol Sci 2018;19:2453.

41. Boone JD, Arend RC, Johnston BE, Cooper SJ, Gilchrist SA, Oelschlager DK, et al. Targeting the Wnt/beta-catenin pathway in primary ovarian cancer with the porcupine inhibitor WNT974. Lab Invest 2016;96:249–59. [PubMed: 26658453]
42. Jiang Y-X, Siu MK-Y, Wang J-J, Mo X-T, Leung TH-Y, Chan DW, et al. Ascites-derived ALDH+CD44+ tumour cell subsets endow stemness, metastasis and metabolic switch via PDK4-mediated STAT3/AKT/NF-kappaB/IL-8 signalling in ovarian cancer. Br J Cancer 2020;123:275–87. [PubMed: 32390009]
43. Ford CE, Werner B, Hacker NF, Warton K. The untapped potential of ascites in ovarian cancer research and treatment. Br J Cancer 2020;123:9–16. [PubMed: 32382112]
44. Flaherty KT, Gray R, Chen A, Li S, Patton D, Hamilton SR, et al. The molecular analysis for therapy choice (NCI-MATCH) trial: lessons for genomic trial design. J Natl Cancer Inst 2020;112:1021–9. [PubMed: 31922567]
45. Verhaak RG, Tamayo P, Yang JY, Hubbard D, Zhang H, Creighton CJ, et al. Prognostically relevant gene signatures of high-grade serous ovarian carcinoma. J Clin Invest 2013;123:517–25. [PubMed: 23257362]
46. Lin J, Kong Q, Hao W, Hu W. High glucose contributes to the polarization of peritoneal macrophages to the M2 phenotype in vivo and in vitro. Mol Med Rep 2020;22:127–34. [PubMed: 32377735]
47. Ren W, Xia Y, Chen S, Wu G, Bazer FW, Zhou B, et al. Glutamine metabolism in macrophages: a novel target for obesity/type 2 diabetes. Adv Nutr 2019;10:321–30. [PubMed: 30753258]
48. Zhang M, He Y, Sun X, Li Q, Wang W, Zhao A, et al. A high M1/M2 ratio of tumor-associated macrophages is associated with extended survival in ovarian cancer patients. J Ovarian Res 2014;7:19. [PubMed: 24507759]
49. Gharpure KM, Lara OD, Wen Y, Pradeep S, LaFargue C, Ivan C, et al. ADH1B promotes mesothelial clearance and ovarian cancer infiltration. Oncotarget 2018;9:25115–26. [PubMed: 29861857]
50. Tanabe S, Quader S, Cabral H, Ono R. Interplay of EMT and CSC in cancer and the potential therapeutic strategies. Front Pharmacol 2020;11:904. [PubMed: 32625096]
51. Nacarelli T, Fukumoto T, Zundell JA, Fatkhutdinov N, Jean S, Cadungog MG, et al. NAMPT inhibition suppresses cancer stem-like cells associated with therapy-induced senescence in ovarian cancer. Cancer Res 2020;80:890–900. [PubMed: 31857293]
52. Kato T, Noma K, Ohara T, Kashima H, Katsura Y, Sato H, et al. Cancer-associated fibroblasts affect intratumoral CD8(+) and FoxP3(+) T cells via IL6 in the tumor microenvironment. Clin Cancer Res 2018;24:4820–33. [PubMed: 29921731]
53. Kaplanov I, Carmi Y, Kornetsky R, Shemesh A, Shurin GV, Shurin MR, et al. Blocking IL-1beta reverses the immunosuppression in mouse breast cancer and synergizes with anti-PD-1 for tumor abrogation. Proc Natl Acad Sci U S A 2019;116:1361–9. [PubMed: 30545915]
54. David J, Dominguez C, Hamilton D, Palena C. The IL-8/IL-8R axis: a double agent in tumor immune resistance. Vaccines 2016;4:22.
55. Teng MWL, Andrews DM, McLaughlin N, von Scheidt B, Ngiow SF, Moller A, et al. IL-23 suppresses innate immune response independently of IL-17A during carcinogenesis and metastasis. Proc Natl Acad Sci U S A 2010;107:8328–33. [PubMed: 20404142]
56. Feng Y, Ren J, Gui Y, Wei W, Shu B, Lu Q, et al. Wnt/beta-catenin-promoted macrophage alternative activation contributes to kidney fibrosis. J Am Soc Nephrol 2018;29:182–93. [PubMed: 29021383]
57. Okamoto A, Nikaido T, Ochiai K, Takakura S, Saito M, Aoki Y, et al. Indoleamine 2,3-dioxygenase serves as a marker of poor prognosis in gene expression profiles of serous ovarian cancer cells. Clin Cancer Res 2005;11:6030–9. [PubMed: 16115948]
58. Raghavan S, Mehta P, Xie Y, Lei YL, Mehta G. Ovarian cancer stem cells and macrophages reciprocally interact through the WNT pathway to promote protumoral and malignant phenotypes in 3D engineered microenvironments. J Immunother Cancer 2019;7:190. [PubMed: 31324218]
59. Wang Y, Cardenas H, Fang F, Condello S, Taverna P, Segar M, et al. Epigenetic targeting of ovarian cancer stem cells. Cancer Res 2014;74:4922–36. [PubMed: 25035395]

60. Jiménez-Sánchez A, Cybulska P, Mager KL, Koplev S, Cast O, Couturier D-L, et al. Unraveling tumor-immune heterogeneity in advanced ovarian cancer uncovers immunogenic effect of chemotherapy. Nat Genet 2020;52:582–93. [PubMed: 32483290]

61. Mesnage SJL, Auguste A, Genestie C, Dunant A, Pain E, Drusch F, et al. Neoadjuvant chemotherapy (NACT) increases immune infiltration and programmed death-ligand 1 (PD-L1) expression in epithelial ovarian cancer (EOC). Ann Oncol 2017;28:651–7. [PubMed: 27864219]

62. Böhm S, Montfort A, Pearce OMT, Topping J, Chakravarty P, Everitt GLA, et al. Neoadjuvant chemotherapy modulates the immune microenvironment in metastases of tubo-ovarian high-grade serous carcinoma. Clin Cancer Res 2016;22:3025–36. [PubMed: 27306793]

63. He Z, Wang X, Zhang H, Liang B, Zhang J, Zhang Z, et al. High expression of folate cycle enzyme MTHFD1L correlates with poor prognosis and increased proliferation and migration in colorectal cancer. J Cancer 2020;11:4213–21. [PubMed: 32368304]

64. Liu X, Gao Y, Lu Y, Zhang J, Li L, Yin F. Downregulation of NEK11 is associated with drug resistance in ovarian cancer. Int J Oncol 2014;45:1266–74. [PubMed: 24969318]

Translational Relevance

Due to the heterogenous nature of ovarian cancer, only homologous recombination status is routinely used to predict clinical outcome and guide treatment. We profiled high-grade serous ovarian cancer (HGSOC) patient tissues using transcriptomic and metabolomic analyses that revealed significant molecular heterogeneity among tumor and ascites derived cells. Our analysis revealed the importance for immune response and WNT signaling in predicting clinical outcomes. These effects could be observed in primary tumor tissue and ascites, although the precise markers were different depending on the tissue source. Altered metabolic profiles were linked to the mesenchymal subtype, which is associated with poor outcomes. We observed strong transcriptional response to treatment with neoadjuvant chemotherapy (NACT) as well as spatial proteomic data that highlighted drug-mediated impacts on both tumors and immune cells. Our work provides a comprehensive view of the dynamic nature of HGSOC, highlighting both candidate biomarkers for predicting patient outcome and potential therapeutic targets.

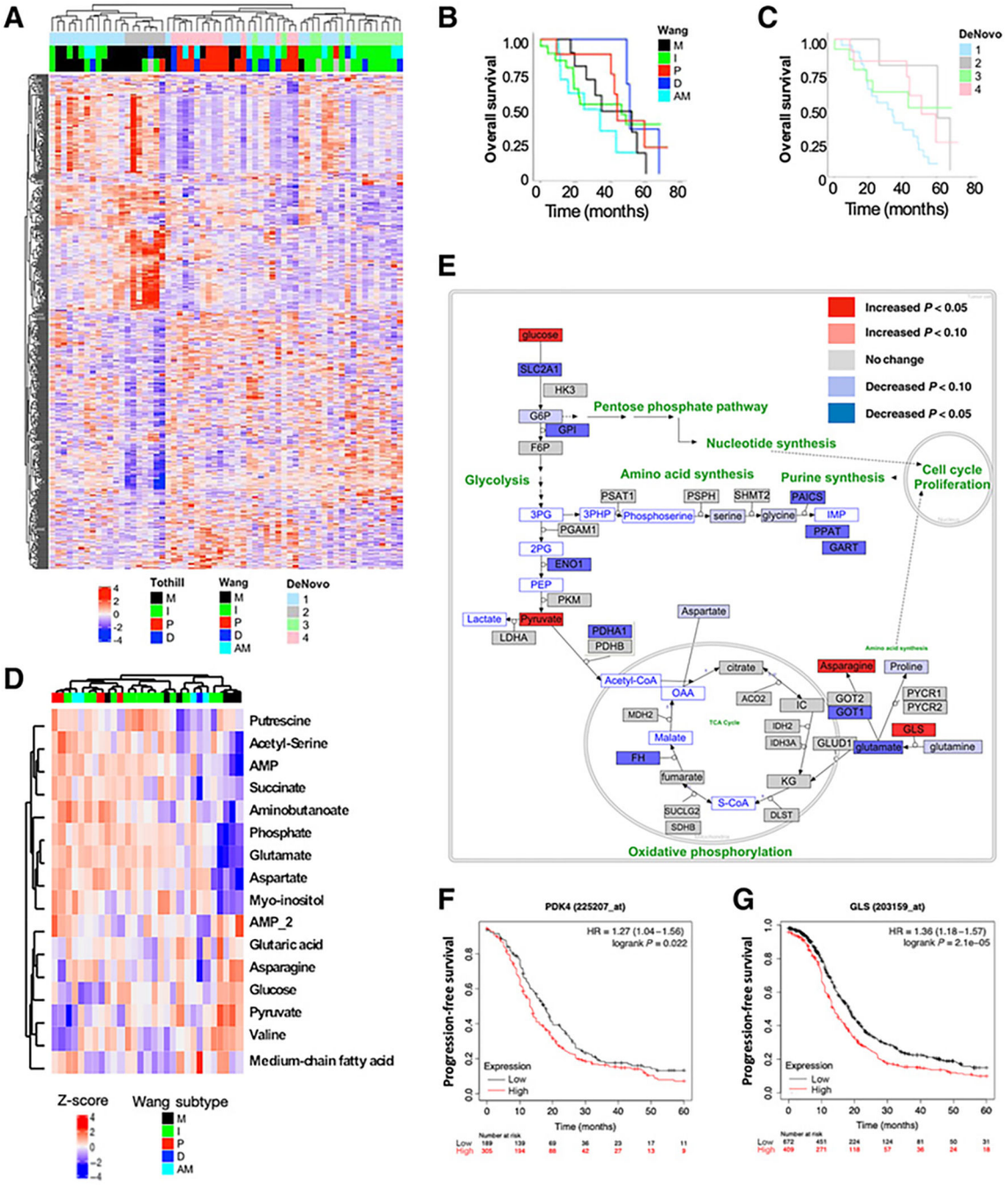

Figure 1.

HGSOC tissues vary from benign and harbor transcriptional and metabolic heterogeneity. Full RNA-seq and pathway analysis was performed on 61 stage IIIC/IV HGSOC patients and 11 benign tissues. **A,** Consensus clustering using the top 1,500 DEGs in HGSOC treatment-naïve tumor tissue defined 4 clusters (DeNovo 1–4), and we compared each cluster's gene expression profile with previously defined transcriptional subtypes (Tothill et al. 2008; Wang et al. 2017). Kaplan–Meier (KM) curves for overall survival (OS) based on Wang-defined (**B**) and DeNovo-defined subtypes (**C**) show no statistical difference in

OS among the subtype groups. Metabolomics data generated by GCxGC-MS is displayed for 30 treatment-naïve HGSOC tissues. **D,** Hierarchical clustering of the top 25 metabolites most different among the five transcriptional subtypes is shown. **E,** An analysis of gene expression and metabolite differences associated with the mesenchymal subtype show significant metabolic changes related to energy metabolism. Glucose, pyruvate, asparagine, and glutaminase (GLS) were among those significantly increased ($P < 0.05$) in the mesenchymal compared with the other subtypes (red). Kaplan–Meier (KM) curves for patient survival based on gene expression of PDK4 (**F**; HR = 1.27, $P = 0.022$) and GLS (**G**; HR = 1.36, $P < 0.001$) in ovarian cancer.

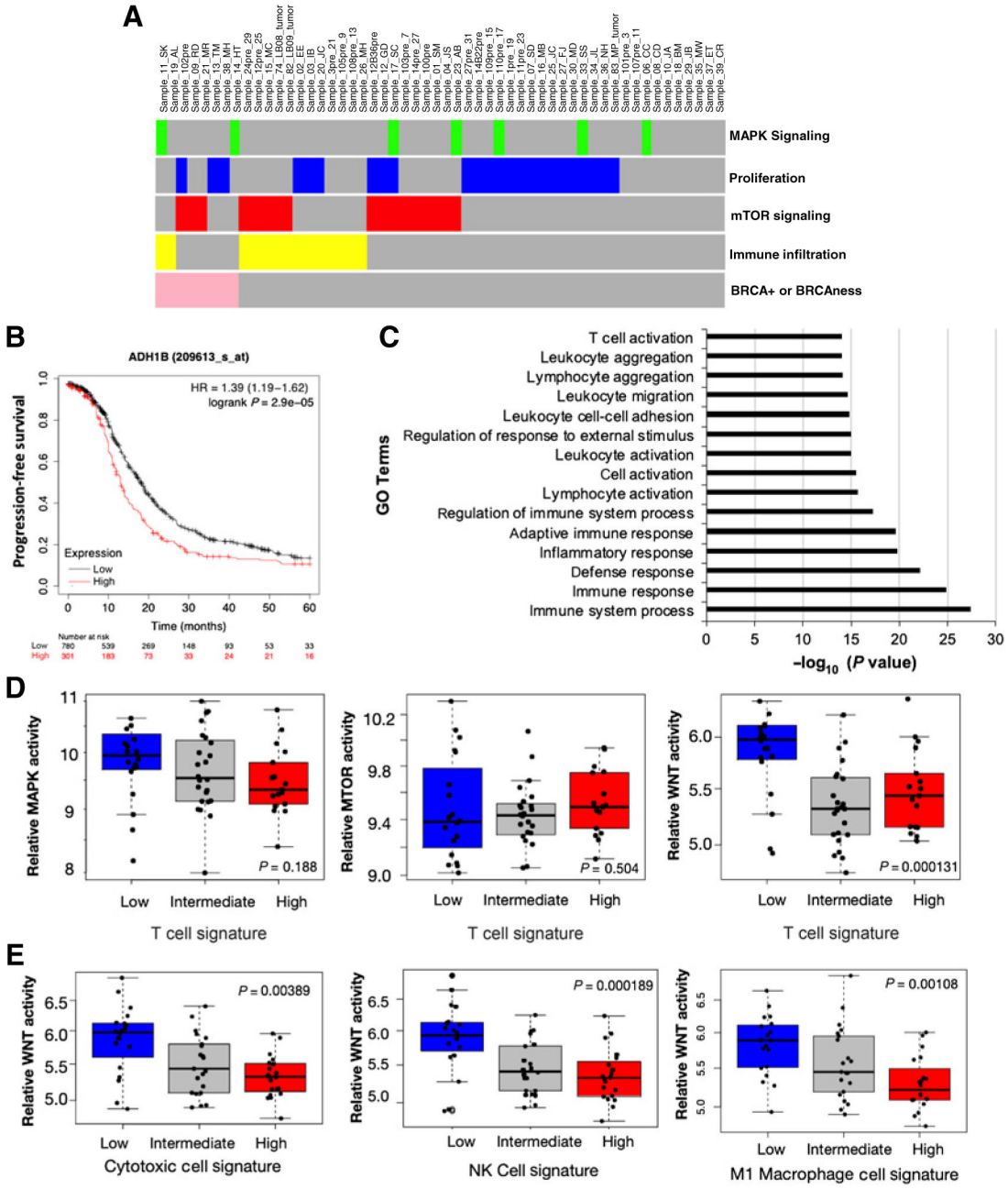

Figure 2.

Identification of genomic features relevant for treatment in tumors. **A,** Transcriptional signatures were used to identify tumor tissues with increased MAPK signaling, proliferation, mTOR signaling, immune infiltration, and BRCAness. Of 61 patients, 14 did not have a gene signature associated with a response to an existing therapy. Analysis of DEGs between these patients and the remaining members of the cohort found an upregulation of *ADH1B* gene (**B**) that corresponds to worse patient prognosis, and pathway analysis revealed that these patients had increased DEGs associated with immune response pathways (**C**). We calculated whether MAPK ($P = 0.188$), mTOR ($P = 0.504$), and/or WNT ($P < 0.001$) signaling were correlated to T-cell infiltration (**D**). **E,** A more detailed analysis of specific

immune cell types showed WNT signaling activity was inversely correlated with infiltration of cytotoxic cells ($P < 0.01$), NK cells ($P < 0.001$), and M1 macrophages ($P < 0.05$).

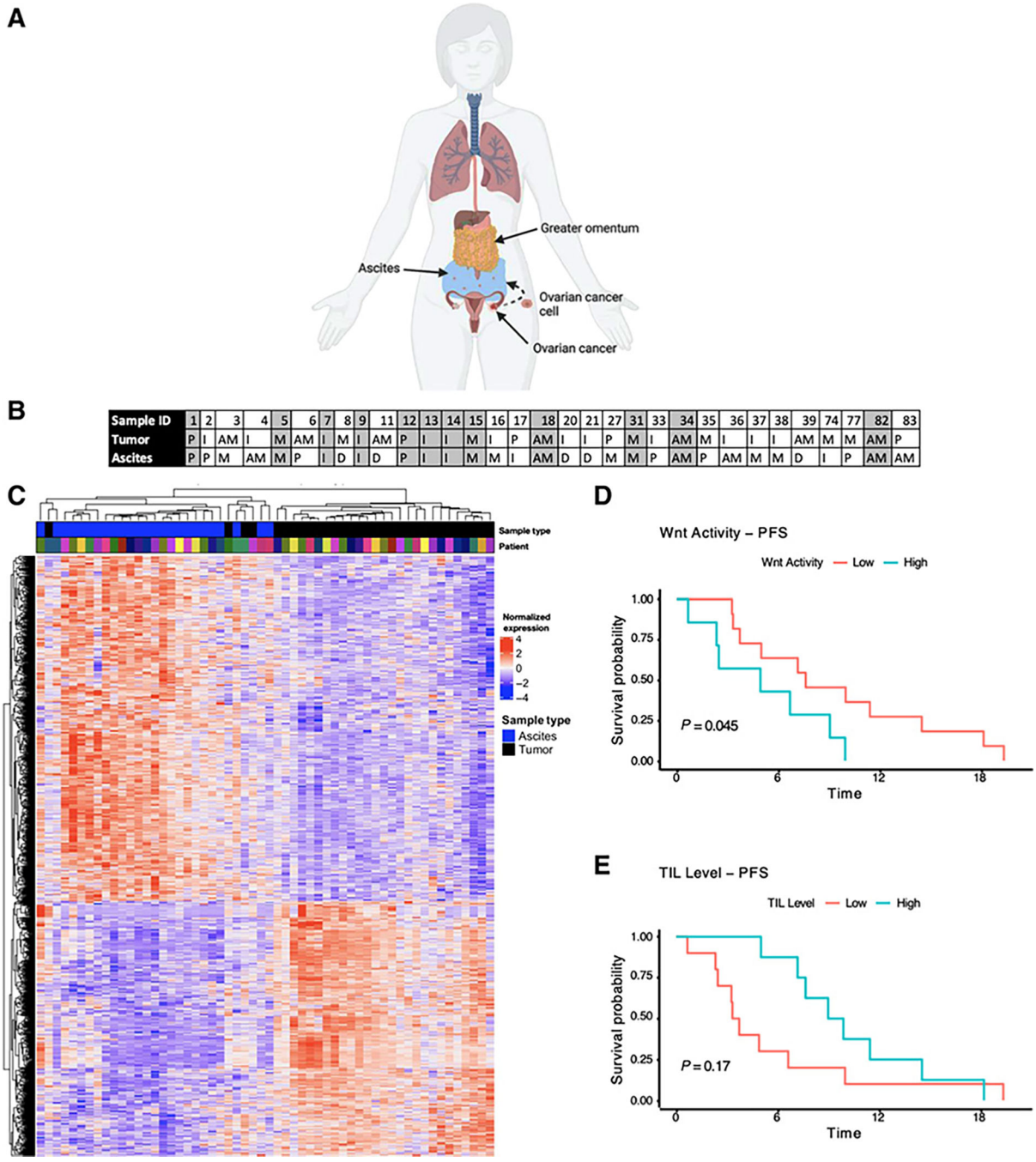

Figure 3.

Variation in gene expression between matched patient tumor and ascites. **A,** Diagram of ovarian cancer primary tumor and ascites cells. **B,** Table of individual patient's primary tumor and ascites transcriptional subtype assignment (Wang et al. 2017). Only 38% ($n = 12$) of patients had the same transcriptional subtype assigned to their primary tumor tissue and ascites. **C,** RNA-seq was performed on 32 patient ascites samples and matched to the same patient's primary untreated tumor tissue. Hierarchical clustering of primary tumor, benign tissue, and ascites cells based on the most variable genes separates benign tissue from tumor

tissue types. Kaplan–Meier (KM) curves showing the effects of WNT pathway activity (**D**) and TIL levels in ascites on progression-free survival of patients with HGSOC (**E**).

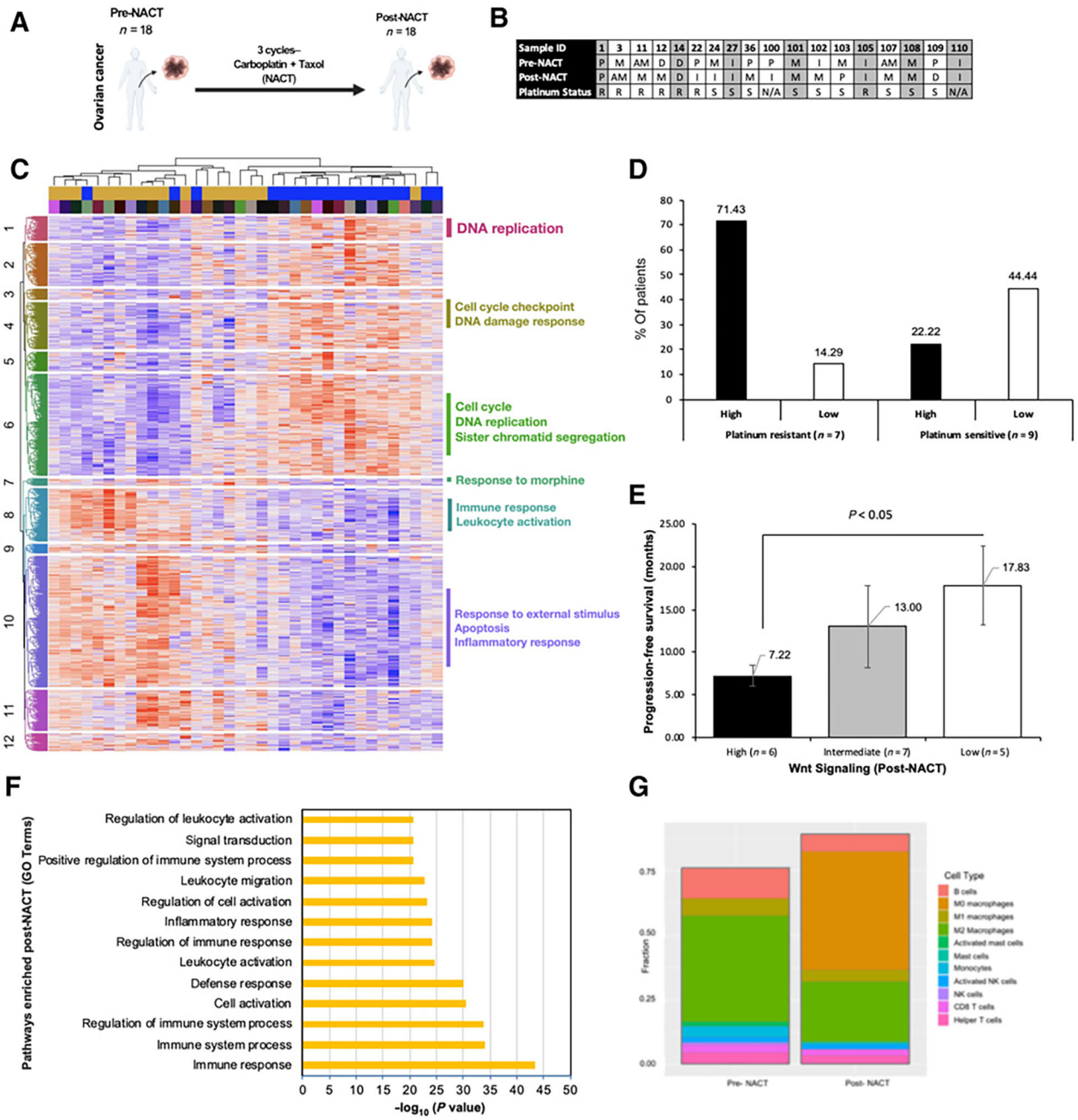

Figure 4.

Transcriptomic analysis of tumors in response to NACT. **A,** We collected samples from 18 patients with matching chemo-naïve tissue (pre-NACT) and tissue collected after 3 to 6 cycles of NACT (post-NACT). **B,** Table of individual patient's (Sample IDs in the first row) pre- and post-NACT tumor transcriptional subtype assignment (Wang et al. 2017). Only 39% ($n = 7$) of patients maintained their transcriptional subtype in response to NACT. Out of the patients whose transcriptional subtype was unchanged 50% were platinum sensitive (PS = S) and 50% were platinum resistant (PR = R). Of the patients whose transcriptional subtype did change, 60% were PS and 40% were PR. **C,** Hierarchical clustering using

all genes with FDR < 0.05 separates pre- and post-NACT samples. **D,** Percentage (%) of patients with high versus low WNT signaling in platinum-resistant versus -sensitive patient groups. **E,** PFS is significantly better in patients whose WNT signaling activity is lower in post-NACT tissue. **F,** Pathway analysis of DEGs identified pathways enriched in post- versus pre-NACT tissues. **G,** Abundance of specific immune cell types compared in pre- and post-NACT tissues.

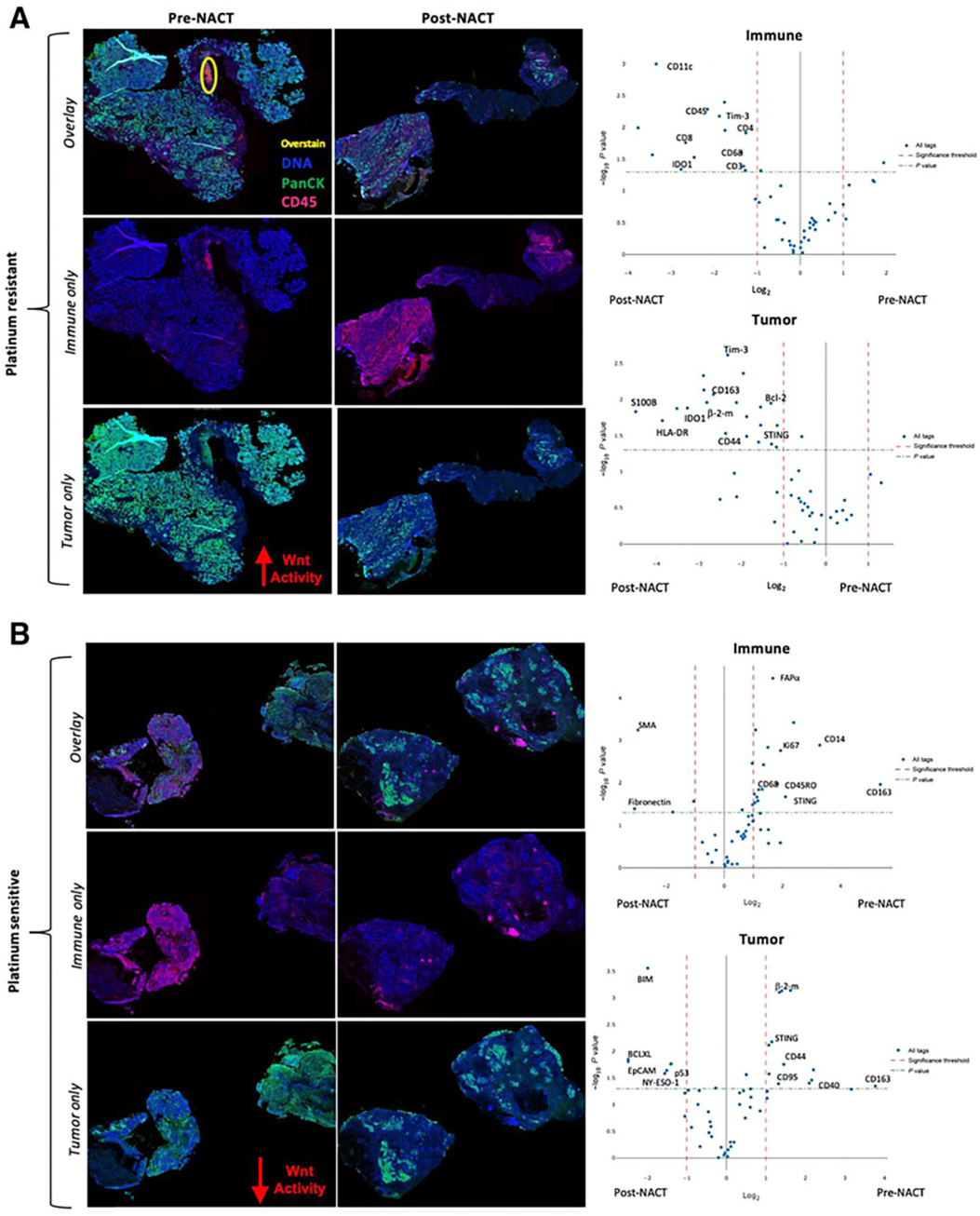

Figure 5.

Proteomic analysis of tumors in response to NACT. Unstained slides from formalin-fixed paraffin-embedded (FFPE) blocks from 2 patients, pre- and post-NACT, were sent for NanoString (https://www.nanostring.com) GeoMx DSP Analysis using the Human Immuno-Oncology Protein Panel. Each slide had 6 ROIs that were segmented into tumor ($PanCK^{+}CD45^{-}$) and immune ($PanCK^{-}CD45^{+}$) areas. **A** and **B,** Platinum resistant (**A**; PR – Sample ID #22 from **B**) and platinum sensitive (**B**; PS – Sample ID #36 from **B**) patient pre- and post-NACT tissue stain and volcano plots representing proteins that were significantly altered in immune and tumor cells specifically in response to NACT.

Table 1.

HGSOC patient demographics.

Total patients	***n* = 61**
Age	
Mean (range)	65 (38–82) years
Body mass index (BMI)	
Mean (range)	28 (18–48)
Race	
White	87% (*n* = 53)
African American	13% (*n* = 8)
Stage	
II	2% (*n* = 1)
III	77% (*n* = 47)
IV	21% (*n* = 13)
Overall survival (OS)	
Mean (range)	35 (0.2–72) months
Progression-free survival (PFS)	
Mean (range)	10 (0–32) months
Treatment strategy	
Primary debulking	70% (*n* = 43)
Neoadjuvant chemotherapy (NACT)	30% (*n* = 18)
BRCA status	
Positive	6% (*n* = 1)
Negative	50% (*n* = 9)
Unknown	44% (*n* = 8)
Platinum sensitivity status	
Sensitive	50% (*n* = 9)
Resistant	39% (*n* = 7)
Unknown	11% (*n* = 2)

Note: Patient age, BMI, race, stage, OS, PFS, treatment strategy, BRCA, and platinum sensitivity status were recorded for each of the 61 patients in our analyses.